Proceedings of the 8th International Symposium on
Spatial Accuracy Assessment in Natural Resources and Environmental Sciences
Shanghai, P. R. China, June 25-27, 2008, pp. 298-304

A New Method for Multi-Temporal SAR Image-Based Change Detection

Juntuan Zhang [1, 2, 3], Shiqi Huang [3 +], Guangliang Zhu [3] and Jun Lin [1]

[1] Texas Instruments-Jilin University DSPs Laboratory, Jilin University, 130026, Changchun, P.R. China
[2] Xi'an Communication Institute, Xi'an, 710106, P.R. China
[3] Xi'an Research Inst. of Hi-Tech, Hongqing Town, Xi'an, 710025, P.R. China

Abstract. Synthetic aperture radar (SAR) imaging has the characteristics of acquiring remote sensing data under all weather and all time. So SAR image change detection techniques have large advantage in abruptly natural and man-made disaster. Inherent speckle noise of SAR image badly obstructs the applications for SAR image change detection. SAR image belongs to non-Gaussian distribution in general, which accords with the conditions of independent component analysis (ICA) theory. The most important benefit is that ICA and wavelet transform both can reduce speckle noise. Therefore, a new change detection algorithm based on ICA and stationary wavelet transform (ICA-SWT-CD) for multi-temporal SAR images was proposed in this paper. The merit of the algorithm is that it is insensitive to speckle noise. Finally, the practical SAR image data is performed compare experiments and the experimental results verify that the proposed algorithm is effective and feasible.

Keywords: SAR image, change detection, independent component analysis, stationary wavelet transform

1. Introduction

SAR can capture remote sensing data under all weather and all time, which can make up for the shortage of optics and infrared remote sensing. Therefore, multi-temporal SAR image change detection is an important content for SAR imaging remote sensing application. SAR image change detection technique is to acquire ground object change information using the same area SAR images at different date and to further realize the qualitative or quantitative analyses of an object. With the development of SAR image technology, multi-platform, multi-band, multi-polarization SAR image resources supply the advantage for change detection. At present, SAR image change detection has been become the issue of remote sensing research and has widely potential applications. In civil field, it can be utilized to disaster surveillance and assessment for the earthquake, flood, mud and rock flow of natural disaster and the big forest fire; it can be used to monitor and survey ocean resource, ocean environment and seaport; it can be used for monitoring and assessment to environmental change and pollution; it can obtain the change information for land utilization, forest and vegetation change, marsh change, city extension, terrain change; it can monitor and evaluate crop growth state; it can update the basic geographic database [1-10]. In military filed, SAR can realize continuous reconnaissance for battlefield area or key monitoring targets; it can be used for target battle damage assessment, battlefield information dynamic perception, monitoring military target and distribution of troops [11, 12].

ICA is a new method for blind source separation in signal processing and data analysis. It is based on the higher-order statistics of signal and can effectively reduce the dependence of second and high-order between multi-source signals. Each component is mutually independent after ICA processing. So ICA plays an important position in image processing. Because ICA has the characteristic that can reduce the correlative

+ Corresponding author. Tel.: +86-29-83348183.
E-mail address: hshiqi@sina.com

ISBN: 1-84626-171-6, **ISBN13:** 978-1-84626-171-8

information among many images, it has been used in remote sensing data transform and analysis, such as the choice and compression of multi-spectral wave band and the classification of multi-spectral images [13-15]. This paper proposes a new algorithm, using wavelet transform and ICA theory to realize the change detection for multi-temporal SAR images.

Firstly, the ICA-SWT-CD algorithm is performed multi-scale decomposition using the two-dimensional discrete stationary wavelet transform (2D-SWT) to multi-temporal SAR images. And a series of high frequency and low frequency sub-images can be obtained, which have the same size with the original SAR images. The optimal wavelet decomposed scale is decided by utilizing comparisons of the local coefficient of variation (LCV) and the global coefficient of variation (GCV). Secondly, the series of sub-images data is transformed into data vector forms and the change areas are obtained by ICA sub-space mapping. Then, the difference vector data into transformed into image data, and they are performed non-coherent weighted sums. Thirdly, the expectation maximization (EM) algorithm is used to confirm the change detection threshold and the changed map is obtained. Finally, the practical multi-temporal SAR images test the proposed approach and the experimental results show the effectiveness.

2. ICA Theory and Fast ICA Algorithm

Jutten C et al firstly presented the concept of ICA in 1988 [16]. The main idea of ICA theory is that data is transformed into mutually independent direction. Every transformed component is not only non-correlative but also mutually independent. Suppose that $x_1(t), x_2(t), \cdots, x_n(t)$ are n dimension observed random variables, and they are the linear combination of n unknown source signals, $s_1(t), s_2(t) \cdots, s_n(t)$. Assume that $x(t) = [x_1(t), x_2(t), \cdots, x_n(t)]^T$, $s(t) = [s_1(t), s_2(t), \cdots, s_n(t)]^T$, after they are combined by the linear mixed system A, they can be expressed by

$$x_i = a_{i1}s_1 + a_{i2}s_2 + \cdots + a_{in}s_n \ ; \quad i = 1, 2, \cdots, m \tag{1}$$

Equation (1) is also written by matrix form, then

$$X = AS = \sum_{i=1}^{n} a_i s_i(t) \tag{2}$$

Where, $A = [a_1, \cdots, a_n]$ is called a mixed matrix, a_i is the base vector of the mixed matrix. Given that each $s_i(t)$ is mutually independent and the problem that ICA will solve is to estimate the unknown and independent source $s(t)$ through another mixed matrix B in terms of observed data $x(t)$.

ICA can estimate the unknown independent source s or mixed matrix A through the observed data X. When ICA estimates source signals, it uses the mixed matrix W. The observed data X is transformed into the output column vector $y(t) = [y_1(t), y_2(t), \cdots, y_n(t)]'$ through W, then

$$Y = WX = WAS \tag{3}$$

The FastICA algorithm finds out one direction through system learning, which is a unit vector W, and makes the projection $W^T x$ have the maximal non-Gaussian. FastICA is based on fixed-point iteration theory, looking for the non-Gaussian maxima of $W^T x$. It only separates one independent component from observed signals every time. Under some optimization of $E\{G(W^T x)\}$, the approximate maxima of $W^T x$ negentropy can be obtained. If the restricted condition is $E\{(w^T x)^2\} = \| w \|^2 = 1$, the optimization of $E\{G(W^T x)\}$ can be got by

$$E\{xg(w^T x)\} - \beta w = 0 \tag{4}$$

Where, the function g is the derivation of G. Using $F(w)$ expresses the left part of the function equation (4), and utilizing Newton iteration method solves equation (4), then its Jacobian matrix $J(w)$ is obtained by

$$J(w) = E[xx^T g'(w^T x)] - \beta I \tag{5}$$

Where, $\beta = E\{w_0^T xg(w_0^T)\}$, moreover

$$E\{xx^T g'(w^T x)\} \approx E\{xx^T\} E\{g'(w^T x)\} = E\{g'(w^T x)\} I \tag{6}$$

Therefore, Jacobian matrix becomes diagonal matrix and it is nonsingular. The approximate Newton iteration formula is gained by

$$w_{k+1} = w_k - \frac{E\{xg(w_k^T x)\} - \beta w_k}{E\{g'(w_k^T x)\} - \beta} \tag{7}$$

Equation (11) is the iteration course of FastICA algorithm [17].

In the course of solving nonlinear equation with Newton iteration, in order to reduce the times of solving Jacobian matrix, the improved Newton iteration method is that Jacobian matrixes of all iterate course take $J(w_0)$ in general. Then the iterative formula is given by

$$w_{k+1} = w_k - F(w_k)/J(W_0) \tag{8}$$

The improved method can save the burden of calculation, but it reduces iterative convergence speed. If the method is used to ICA, it may even result in that the algorithm can't converge finally. Therefore, the application of the method is not ideal. The following improved method can greatly reduce iterative times and does not increase the times of solving Jacobian matrix. So it reduces the burden of calculation and increases the convergent effect. Assume that w_k has been solved, and w_{k+1} can be obtained by following equation, which is given by

$$w_k^{(0)} = w_k;\ \ w_k^{(i)} = w_k^{(i-1)} - \frac{F\{w_k^{(i-1)}\}}{J\{w_k^{(i-1)}\}}; (i = 1,2,\cdots,m);\ \ w_{k+1} = w_k^{(m)} \tag{9}$$

The convergent order of equation (9) is $m+1$, and it only needs computing one time $J(w)$ in every m times iteration. Therefore, it reduces the burden of calculation and improves iteration speed. When $m = 2$, equation (9) can be simplified as

$$w_{k+1} = w_k - \frac{F(w_k) + F\{w_k - F(w_k)/J(w_k)\}}{J(w_k)} \tag{10}$$

What $F(w_k)$ and $J(w_k)$ describe is taken into equation (10), the iteration course of M-FICA algorithm can be got. The basic format of M-FICA algorithm as follows

(1) Choose initial random weight vector w_0.

(2) Using equation (10) updates w_{k+1}.

(3) Normalize w_{k+1}, $w_{k+1} = \frac{w_{k+1}}{\| w_{k+1} \|}$.

(4) If $| w_{k+1} - w_k | > \varepsilon$, the algorithm is not convergent, then return the step (2), otherwise, estimate an independent component and the algorithm finishes.

For multi-independent component being obtained, it only needs to repeatedly use the basic format of M-FICA. But after one component is extracted every time, the independent component needs to be subtracted from the observed signals. In such a way, repeatedly perform until all independent components are extracted. The method taking out those extracted independent components is given by

$$w_{k+1} = w_{k+1} - \sum_{j=1}^{k} w_{k+1}^T w_j w_j;\ \ w_{k+1} = \frac{w_{k+1}}{\sqrt{w_{k+1}^T w_{k+1}}} \tag{11}$$

3. Description of ICA-SWT-CD Algorithm

The principle of the ICA-SWT-CD algorithm for SAR images is subspace mapping and multi-scale decomposing, and the flow chart of it is shown in Fig. 1. Suppose that the corresponding SAR images of time t_1 and t_2 are X_1 and X_2, respectively. If the independent component S_1 of X_1 can be estimated, X_2 will be mapped to subspace of X_1 by the subspace mapping method. The difference that is obtained between the mapped signal X_1' and original signal X_2 may detect the changes that signal X_2 is relative to signal X_1. The subspace mapping mixed matrix A_{21} from X_2 to X_1 is given by

$$A_{21} = X_2 * pinv(S_1) \tag{12}$$

Where *pinv* denotes pseudo-inverse operation, $*$ denotes matrix multiplicative operation. The mapping from X_2 to X_1 can be expressed by

$$X_2' = A_{21} * S_1 \tag{13}$$

The changes that X_2 is relative to X_1 can be expressed by

$$D_{X_2 \to X_1} = X_2 - X_2' \tag{14}$$

With the same way, we can also obtain the changes $D_{X_1 \to X_2}$ that X_1 is relative to X_2.

It is shown in Fig. 1 that the key techniques of the ICA-SWT-CD algorithm for SAR images are wavelet multi-scale decomposition and ICA subspace extraction. The confirmation of the decomposed scale is the key step of wavelet transform. This paper uses the comparison of LCV and GCV to confirm wavelet decomposed scale. For image data matrix, because of iterative complexity of the ICA algorithm, we need to transform image data matrix and perform independent component extraction. Usual transform method is to make even block to an image. Different block methods cause the different extent changes for detected results, such as the sizes and directions of blocks different, and it is very difficult to obtain the optimal results. Therefore, this paper proposes using the two-dimensional discrete stationary wavelet transform (2D-SWT) to decompose different temporal SAR images, instead of the standard discrete wavelet transform (DWT). This is because the sub-images decomposed by 2D-SWT have the same size like the original images at every resolution layer, which is not like the DWT. 2D-SWT avoids down-sampling the filtered signals. The 2D-SWT decomposition preserves translation invariance and allows avoiding aliasing effects during synthesis without providing high-frequency components. At the same time, it fully plays the characteristics of wavelet transform orthogonality and directionality, which make the combination of data block to be optimized.

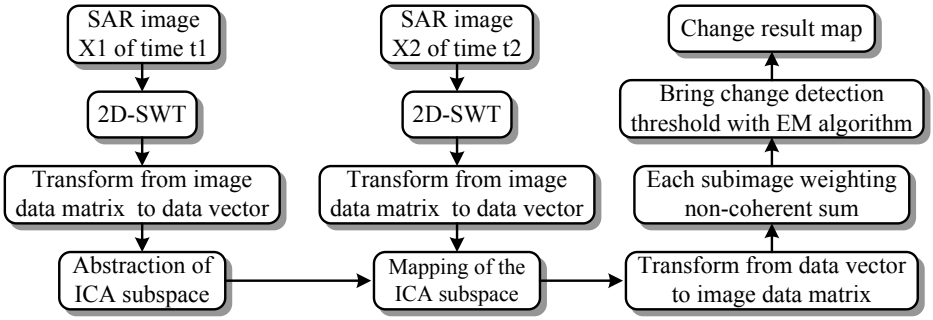

Fig. 1 The flow chart of SAR image change detection algorithm based on ICA and wavelet transform

According to Fig. 1, the ICA-SWT-CD algorithm for SAR images mainly includes the following steps.

(1) Perform 2D-SWT multi-scale decompose to multi-temporal SAR images.

The key step of wavelet transform is the confirmation of multi-scale decomposed level M, which is determined by LCV and GCV. A series of sub-images X_{MS} can be obtained after the SAR image X_1 is decomposed by 2D-SWT and the definition is given by

$$X_{MS} = \{X_1^0, \cdots, X_1^n, \cdots, X_1^{N-1}\} \tag{15}$$

Where, the superscript n $(n = 0,1,\cdots,N-1)$ indicates the resolution level. In a given scale n, that a pixel belongs to border or homogeneous area is decided by using a multi-scale local coefficient of variation (LCV^n). The coefficient of variation (CV) is an index to describe the local non-homogeneous degree of SAR images, and it also act as a theoretical value which reflects amount of speckle noise. The definition of LCV^n is given by

$$LCV^n(i,j) = \frac{\sigma^n(i,j)}{m^n(i,j)} \tag{16}$$

Where $\sigma^n(i,j)$ and $m^n(i,j)$ are the local standard deviation and the local mean, respectively. Using the equation (16) computes the LCV of the spatial position (i,j) at the resolution level n $(n = 0,1,\cdots,N-1)$. In order to improve the precision, a moving window is adopted while computing LCV in general, and the size of the moving is defined by users. If the size of the moving window is too small reduces the reliability of the local statistical parameters, while windows that are too large decrease in sensitivity to identify geometrical details. Therefore, the selected size should be a tradeoff between the above properties. CV is a measure of the scene heterogeneity. Low values correspond to homogeneous areas, while high values refer to heterogeneous areas (e.g., border areas and point targets). For separating the homogeneous from the

heterogeneous regions, we must define a threshold value. In resolution level n, the homogeneity degree of a homogeneous region can be expressed in relation to the global coefficient of variation (GCV^n) of the considered image. It is defined by

$$GCV^n = \sigma^n / m^n \tag{17}$$

Where σ^n and m^n are the standard deviation and the mean computed over a homogeneous region at resolution level n, respectively. In every scale, the homogeneous regions can be decided by those regions that satisfy the following condition.

$$LCV^n(i,j) \le GCV^n \tag{18}$$

For a given pixel, if it satisfies the equation (18) in all resolution levers t $(t = 0,1,\cdots,r)$, the resolution level $r(r = 0,1,\cdots,N-1)$ is said to be reliable. For a pixel (i,j), the set of images with reliable scale is defined by

$$X_{MS}^{R_{ij}} = \left\{ X_1^0, \cdots, X_1^n, \cdots X_1^{S_{ij}} \right\}, \qquad S_{ij} \le N-1 \tag{19}$$

Where S_{ij} is the level with the lowest resolution (identified by the highest value n). The pixel (i,j) can be represented without any border problems and therefore it satisfies the definition of reliable scale.

(2) Image data matrixes transform into data vectors.

After the SAR image X_1 at time t_1 is decompose by wavelet, a series of low frequency sub-images C_{1i} and high frequency sub-images D_{1i}^1, D_{1i}^2 and D_{1i}^3 are obtained. Then they compose the block vector X_{1T}. With the same way, the block vector X_{2T} can be obtained to SAR image X_2 at time t_2. They are given by

$$\begin{cases} X_{1T} = \left[C_{1i}, D_{11}^1, D_{11}^2, D_{11}^3, \cdots, D_{1i}^1, D_{1i}^2, D_{1i}^3 \right]^T \\ X_{2T} = \left[C_{2i}, D_{21}^1, D_{21}^2, D_{21}^3, \cdots, D_{2i}^1, D_{2i}^2, D_{2i}^3 \right]^T \end{cases} ; \quad i = 0,1,\cdots,r \tag{20}$$

Where, i indicates the decomposed level, r indicates the stable multi-scale decomposed level. Equation (20) shows that the essential of making image blocks with wavelet transform is results that low and high frequency components after wavelet transform at all stabile level are spread to one data row vector.

(3) Using subspace mapping algorithm realizes the changed areas extraction.

The changed areas can be obtained in terms of equation (12), equation (13) and equation (14), namely

$$D_{X_{2r} \to X_{1r}} = X_{2T} - X'_{2T} \tag{21}$$

(4) The changed area vector data is transform into image data matrixes.

(5) All image data matrixes perform weighting non-coherent sum X_D.

(6) Using EM algorithm performs operations to image X_D and the change detection judgment threshold T is obtained.

(7) The final changed map is obtained.

4. Experimental Results and Analysis

Experimental data comes from airborne C/X-SAR remote sensing data of Canada Centre for Remote Sensing (CCRS). The original images are shown in Fig. 2. Where, Fig. 2(a) and Fig. 2(b) are single SAR images at different date, which are C wave band HH polarization image and the spatial resolution is $5m \times 5m$. The imaging dates of Fig. 2(a) and Fig. 2 (b) are Mar. 18, 1991 and Feb. 8, 1992, respectively. Suppose that Fig. 2(a) is X_1 at time t_1 and Fig. 2(b) is X_2 at time t_2, and they are revised by radiation and geometry and registration. The area is a piece of forest. Because the frost is fallen, the ground object class changes, but its scattering structures don't change. This leads to change for the final SAR image. The scattering intensity of forest is stronger than that of the bare ground surface. So after the forest is fallen, the backscattering intensity becomes weak. In SAR image, it indicates dark, which is shown in Fig. 2(b). The brighter line area in the center of Fig. 2(b) is dihedral reflection effect between ground surface and forest. It belongs to strong scattering structure and the echo intensity is stronger, so it is brighter in SAR image.

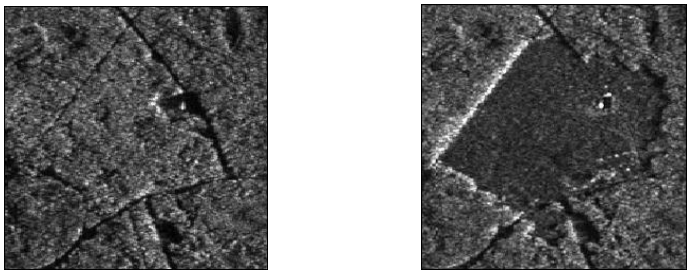

(a) Before change (b) After change

Fig. 2 SAR images before change and after change

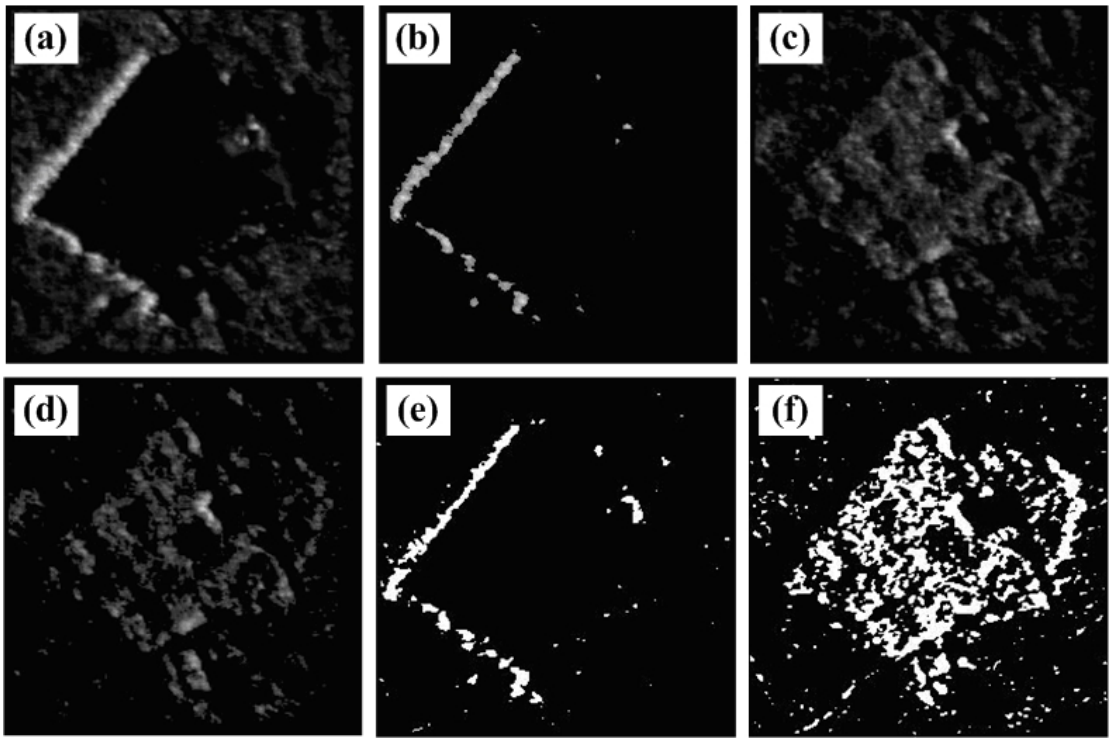

Fig. 3 The compression of detection results

In order to test the validity of the new algorithm which is proposed by this paper, we make compare experiments and experimental results are shown in Fig. 3. The experimental methods are the ICA-SWT-CD algorithm and image grey difference change detection algorithm. Where, Fig. 3(a), Fig. 3(b), Fig. 3(c) and Fig. 3(d) are the experiments with the new algorithm. Fig. 3(e) and Fig. 3(f) are the experiments with the image grey difference algorithm. Fig. 3(a) is the changed area image which X_2 is relative to X_1 and Fig. 3(b) is the change detection results of Fig. 3(a). Fig. 3(c) is the changed area image which X_1 is relative to X_2 and Fig. 3(d) is the change detection results of Fig. 3(c). Fig. 3(e) is the change-enhanced area image with image grey difference method and Fig. 3(f) is the change-weakened area image with image grey difference method. It is seen from Fig. 3 that the new method can effectively detect SAR changed area and the detection effect is close to the results of image grey difference algorithm. This verifies that the ICA-SWT-CD algorithm is feasible.

5. Conclusions

Aiming at inherent speckle noise of SAR images, a new SAR image change detection algorithm is proposed, which is called the ICA-SWT-CD algorithm. It is insensitive to speckle noise. Some real SAR image data performs according to experiments. Experimental results show that the ICA-SWT-CD algorithm is effective. Because ICA is high order statistical method, it may be spread to more dimension data and image sequence analysis, which can satisfy the requirement of image change detection. So it has some theoretical and practical significance.

6. References

[1] S. Quegan, T. Le Toan, J. J. Yu, F. Ribbes, and N. Floury, Multitemporal ERS SAR analysis applied to forest mapping, *IEEE Transactions on Geoscience and Remote Sensing*, 2000, **38**(2): 741-753.

[2] K. Grover, S. Quegan, and C. da Costa Freitas, Quantitative estimation of tropical forest cover by SAR, *IEEE Transactions on Geoscience and Remote Sensing*, 1999, **37**(1): 479-490.

[3] L. Bruzzone and S. B. Serpico, An iterative technique for the detection of land-cover transitions in multispectral remote-sensing images, *IEEE Transactions on Geoscience and Remote Sensing*, 1997, **35**(4): 858-867.

[4] S. Henning, T. S. Morten and G. T. Anton, Multitemporal C- and L-Band polarimetric signatures of crops, *IEEE Transactions on Geoscience and Remote Sensing*, 1999, **37**(5): 2413-2429.

[5] K. R. Merril and L. Jiajun, A comparison of four algorithms for change detection in an urban environment, *Remote Sensing Environment*, 1998, **63**(2): 95-100.

[6] T. T. Lee and R. Florrence, Rice crop and monitoring using ERS-1 data based on experiment and modeling results, *IEEE Transactions on Geoscience and Remote Sensing*, 1997, **35**(1): 41-55.

[7] H. Zhang, N. Hu and G. Liu, Application of multitemporal composition and classification to land use change detection, *Geomatics and Information Science of Wuhan University*, 2005, **30**(2): 131-134.

[8] J. F. Zhang, L. L. Xie and X. X Tao, Change detection of remote sensing image for earthquake-damaged buildings and its application in seismic disaster assessment, *Chinese Journal of Natural Disasters*, 2002, **11**(2): 59-64.

[9] B. Mansouri, *Remote sensing: feasibility of change/damage detection in urban areas and structures by synthetic aperture radar (SAR) Imagery*, University of Southern California, the Graduate School University Park Los Angeles, California, 2002.

[10] G. Paolo, D. A. Fabio and T. Giovanna, Rapid damage detection in the bam area using multitemporal SAR and exploiting ancillary data, *IEEE Transactions on Geoscience and Remote Sensing*, 2007, **45**(6): 1582-1589.

[11] W. X. Fu, S. H. Li and W. Hong, Hitting effect evaluation based on high-resolution SAR images, *ACTA ELECTRONICA SINICA*, 2003, **31**(9): 1290-1294.

[12] S. Q. Huang, D. Z. Liu and L. Chen, A study of the damage detection method for smooth earth surface, *Chinese Journal of Geophysics*, 2007, **50**(4): 315-321.

[13] Y. S. Fu, Y. Xie, Y. M. Pi and Y. M. Hou, Unsupervised classification of polarimetric synthetic aperture radar images based on independent component analysis, *Chinese Journal of Radio Science*, 2007, **22**(2): 255-260.

[14] J. Ji and Z. Tian, New speckle reduction method for polarimetric SAR image based on independent component analysis, *Chinese Computer Applications*, 2006, **26**(1): 2354-2356.

[15] Z. Y. Su and A. L. Chen, The independent component analysis and its application in the geographical and environmental fields, *Journal of Chongqing Normal University (Natural Science Edition)*, 2005, **22**(4): 16-20.

[16] C. Jutten and J. Herault, Independent component analysis verus principal component analysis, *Proceeding Europe Signal Processing Conference*, EUSIPC088, 1988: 643-646.

[17] A. Hyvarinen, Fast and robust fixed-point algorithms for independent component analysis, *IEEE Trans on Neural Networks*, 1999, **8**(3): 622-634.